



Diamagnetism and Cooper pairing above T_c in cuprates

Lu Li,¹ Yayu Wang,^{1,2} Seiki Komiya,³ Shimpei Ono,³ Yoichi Ando,^{3,4} G. D. Gu,⁵ and N. P. Ong¹

¹*Department of Physics, Princeton University, Princeton, New Jersey 08544, USA*

²*Department of Physics, Tsinghua University, Beijing, China*

³*Central Research Institute of Electric Power Industry, Komae, Tokyo 201-8511, Japan*

⁴*Institute of Scientific and Industrial Research, Osaka University, Ibaraki, Osaka 567-0047, Japan*

⁵*Brookhaven National Laboratory, Upton, New York 11973, USA*

(Received 13 July 2009; revised manuscript received 8 December 2009)

In the cuprate superconductors, Nernst and torque magnetization experiments have provided evidence that the disappearance of the Meissner effect at T_c is caused by the loss of long-range phase coherence, rather than the vanishing of the pair condensate. Here we report a series of torque magnetization measurements on single crystals of $\text{La}_{2-x}\text{Sr}_x\text{CuO}_4$ (LSCO), $\text{Bi}_2\text{Sr}_{2-y}\text{La}_y\text{CuO}_6$ (Bi 2201), $\text{Bi}_2\text{Sr}_2\text{CaCu}_2\text{O}_{8+\delta}$, and optimal $\text{YBa}_2\text{Cu}_3\text{O}_7$. Some of the measurements were taken to fields as high as 45 T. Focusing on the magnetization above T_c , we show that the diamagnetic term M_d appears at an onset temperature T_{onset}^M high above T_c . We construct the phase diagram of both LSCO and Bi 2201 and show that T_{onset}^M agrees with the onset temperature of the vortex Nernst signal T_{onset}^v . Our results provide thermodynamic evidence against a recent proposal that the high-temperature Nernst signal in LSCO arises from a quasiparticle contribution in a charge-ordered state.

DOI: XXXX

PACS number(s): 74.25.Dw, 74.25.Ha, 74.72.-h

I. INTRODUCTION

A series of experiments utilizing the Nernst effect¹⁻⁵ has demonstrated that an enhanced Nernst signal is observed in hole-doped cuprates at temperatures T significantly above the superconducting transition temperature T_c . The high- T Nernst region was identified as a continuous extension of the vortex-liquid state. In this strongly fluctuating vortex-liquid state, the large Nernst signal arises from phase slippage caused by singular phase fluctuations of the pair condensate.^{2,5} In the phase-disordering scenario, the unbinding of vortex-antivortex pairs (in zero applied H) leads to the loss of long-range phase coherence at T_c .⁶ The condensate is incapable of displaying long-range supercurrent response. Hence, even in weak H , there is no Meissner effect above T_c despite the survival of the pair condensate. Nevertheless, the persistent short-range phase stiffness supports vorticity and produces a large, strongly T -dependent Nernst signal in the presence of a temperature gradient $-\nabla T$ and an applied magnetic field \mathbf{H} . The Nernst effect above T_c has also been investigated in Refs. 7-9.

Subsequently, thermodynamic evidence for the pair condensate above T_c was obtained by torque magnetometry, which is a very sensitive probe of diamagnetism in the cuprates.^{10,11} A large diamagnetic response, that is nonlinear in H and grows strongly with decreasing T , is specific to the Cooper-pair condensate. Consequently, the diamagnetism results present clear evidence for survival of the pair condensate, with sharply reduced phase stiffness, to temperatures high above T_c . This complements the transport evidence from the Nernst experiments. To date, the high-resolution torque measurements above T_c have been reported in the bilayer cuprate $\text{Bi}_2\text{Sr}_2\text{CaCu}_2\text{O}_{8+\delta}$ (Bi 2212) (Refs. 10-14) and in lightly doped $\text{La}_{2-x}\text{Sr}_x\text{CuO}_4$ (LSCO) at low T .¹⁵ For earlier measurements of diamagnetism above T_c , see Ref. 16 (on Bi 2212) and Ref. 17 (LSCO).

We report further torque magnetization experiments on $\text{La}_{2-x}\text{Sr}_x\text{CuO}_4$, $\text{Bi}_2\text{Sr}_{2-y}\text{La}_y\text{CuO}_6$, $\text{Bi}_2\text{Sr}_2\text{CaCu}_2\text{O}_{8+\delta}$, and

$\text{YBa}_2\text{Cu}_3\text{O}_7$ (YBCO), which show that, when a positive Nernst signal appears below the onset temperature T_{onset} , it is accompanied by a large diamagnetic signal that grows steeply with decreasing T . Extending the torque measurements to intense fields (33-45 T), we also show that the curves of M vs H are nonlinear with a profile characteristic of vortex-liquid response, even at elevated T .

Recently, the fluctuating vortex-liquid interpretation of the Nernst effect has been challenged by Cyr-Choiniere *et al.*,¹⁸ who carried out Nernst measurements on a series of Nd- and Eu-doped LSCO cuprates, in which charge ordering associated with stripe formation is known to occur at a charge-ordering temperature T_{CO} . By a qualitative comparison of the Nernst coefficient ν in Nd-LSCO and Eu-LSCO, Cyr-Choiniere *et al.* proposed that, in pure LSCO, the high-temperature Nernst signal e_N arises from small quasiparticle (qp) pockets as a result of Fermi-surface (FS) rearrangement, rather than from phase slippage in the pair condensate. We discuss the problem of separating the vortex Nernst term from quasiparticle contributions and the key role that diamagnetism plays in this task. In pure LSCO, we explain how the magnetization results reported here pose serious difficulties for this hypothesis.

We adopt the abbreviations LSCO 09, LSCO 12, and LSCO 17 for $\text{La}_{2-x}\text{Sr}_x\text{CuO}_4$ with the Sr content $x=0.09$, 0.12, and 0.17, respectively. We use Bi 2201 and Bi 2212 to stand for $\text{Bi}_2\text{Sr}_{2-y}\text{La}_y\text{CuO}_6$ and $\text{Bi}_2\text{Sr}_2\text{CaCu}_2\text{O}_{8+\delta}$, respectively, and YBCO for $\text{YBa}_2\text{Cu}_3\text{O}_7$. The terms underdoped, optimally doped, and overdoped are abbreviated as UD, OPT, and OV, respectively.

II. TORQUE MAGNETOMETRY

The torque magnetization was measured with the sample glued to the tip of a thin cantilever with \mathbf{H} applied at a tilt angle $\theta=10^\circ-15^\circ$ to the crystal c axis. The deflection φ of

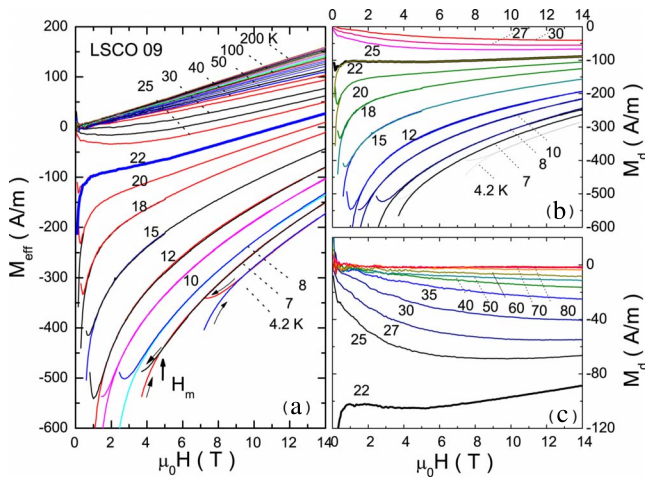


FIG. 1. (Color online) Magnetization curves of sample LSCO 09 with Sr content $x=0.09$ and transition temperature $T_c=24$ K measured in magnetic fields H up to 14 T. (a) The (total) effective magnetization M_{eff} vs H at temperatures $4.2 \leq T \leq 200$ K. Below T_c , the M_{eff} - H curves are hysteretic when H lies below the melting field $H_m(T)$, which is experimentally defined as the field at which the up-sweep branch deviates from the down-sweep branch (H_m is indicated by an arrow for the curve at 7 K). Above H_m , the curves become reversible. (b) The diamagnetic magnetization M_d vs H at temperatures $4.2 \leq T \leq 30$ K. (c) Curves of M_d vs H at $22 \leq T \leq 80$ K displayed in expanded scale. In LSCO 09, the diamagnetic signal persists to more than 60 K above T_c . In (b) and (c), the bold curve is measured at the separatrix temperature $T_s=22$ K.

tion of the paramagnetic Van Vleck term. At $T < T_c$, the M_{eff} - H curves at low fields display strong hystereses between up-sweep and down-sweep branches because of strong pinning in the vortex-solid state. In the plotted curves, this is seen as a fork (we suppress the full hysteretic curves in both branches for clarity). The field at which the down-sweep branch deviates from the up-sweep branch is experimentally defined as the melting field $H_m(T)$ of the vortex solid (indicated by arrow for the curve at 7 K). As T is raised, H_m decreases rapidly, reaching zero at T_c . A detailed investigation of $H_m(T)$ in lightly doped LSCO is reported in Ref. 15. The spin contribution to M_{eff} , which becomes important below 2 K in samples with $x < 0.06$, is also treated in detail in Ref. 15.

We assume that the paramagnetic background $\Delta\chi_p H$ follows the trend that is seen at $T > T_{onset}$. Hence the diamagnetic term M_d is related to the observed torque magnetization M_{eff} by

$$M_{eff}(H) = M_d + \Delta\chi_p(T)H = M_d(H) + (A + BT)H. \quad (1)$$

Hereafter, we subtract the background Van Vleck term $(A + BT)H$ from M_{eff} and plot the diamagnetic term M_d vs H (except stated otherwise).

III. LSCO

Carrying out the background subtraction for LSCO 09, we obtain the M_d vs H curves. They are displayed at selected T in Fig. 1(b) (4.2–30 K) and Fig. 1(c) (20–80 K). As shown in panel (b), M_d is nonlinear in H over a broad temperature interval. The curve at 22 K (bold curve) displays a characteristic flat profile in low fields ($0.5 < H < 5$ T). We identify this temperature as the “separatrix” temperature T_s . Below T_s , M_d takes on very large, negative values at small H . As H increases, M_d displays an initially steep logarithmic increase, followed by a slower approach toward zero as H approaches the upper critical field H_{c2} . The low-field curvature of the M_d vs H curve changes from negative below T_s to positive above T_s . To emphasize the high-temperature diamagnetic response, panel (c) displays the M_d - H of sample LSCO 09 at $T \geq T_s$ in expanded scale. For $T > T_s$, the curves remain diamagnetic, displaying pronounced nonlinearity vs H . We regard the nonlinear diamagnetic response above T_c as clear evidence for the presence of local supercurrents as well as finite pair amplitude in the pseudogap state.

As in the superconducting state, the diamagnetic signals above T_c can be suppressed by an intense magnetic field. To get a sense of how large this field scale is, we extended the torque measurements on LSCO 09 to 33 T. After the background subtraction described above, the resulting M_d - H curves are isolated and plotted in Fig. 2. For $T > T_c$, these nonlinear M_d - H curves display a broad minimum. The characteristic field H_{min} locating the minimum increases rapidly with T (from 8 T at 25 K to 33 T at 40 K). A rough measure of the field scale needed to observe the inherent nonlinear response above T_c is given by H_{min} .

We emphasize that, above 50 K, M_d is seemingly linear in H . However, this is simply because H_{min} has now moved outside the experimental window. It is incorrect to attribute,

93 the cantilever by the torque was detected capacitively. The
 94 cantilever typically can resolve changes in the magnetic moment of $\delta m \sim 10^{-9}$ emu. Because of the two-dimensional
 95 (2D) electronic dispersion in cuprates, the diamagnetic orbital currents are largely confined to the a - b plane.^{10,19} This
 96 makes torque magnetometry well suited for detecting weak,
 97 incipient diamagnetism in cuprate crystals. We generally report the raw data as the effective torque magnetization M_{eff}
 98 defined as $M_{eff} = \tau / \mu_0 H V \sin \theta$, where τ is the torque signal, μ_0 the vacuum permeability, and V the sample volume. (M_{eff}
 99 includes all contributions to the observed torque signal.)
 100 To describe our analysis, we first examine the curves of
 101 M_{eff} vs H shown in Fig. 1(a) for sample LSCO 09 with T_c
 102 = 24 K. At temperatures $T > 100$ K, M_{eff} is strictly linear in
 103 H and paramagnetic in sign. This reflects the dominance of
 104 the anisotropic Van Vleck paramagnetic susceptibility $\Delta\chi_p$,
 105 which has a weak T dependence given by $\Delta\chi_p = A + BT$, with
 106 $A \gg BT > 0$ at 200 K. (The T dependence of M_{eff} will be
 107 shown later in Fig. 9.) The reason for measuring a dense set
 108 of curves in the high- T interval 100–200 K will emerge when
 109 we discuss extraction of the onset temperature for diamagnetic
 110 response (Sec. VI). Below 100 K, M_{eff} begins to display a weak
 111 diamagnetic contribution that rapidly increases in magnitude as T
 112 decreases. The temperature at which the diamagnetic contribution (referred to as M_d hereafter) appears is identified as the onset temperature T_{onset}^M .
 113 We note that M_{eff} becomes increasingly nonlinear in H as
 114 T decreases from 60 K to T_c (24 K). Below T_c , the diamagnetic
 115 term becomes so dominant in magnitude that M_{eff} is
 116 forced to large, negative values despite the positive contribu-

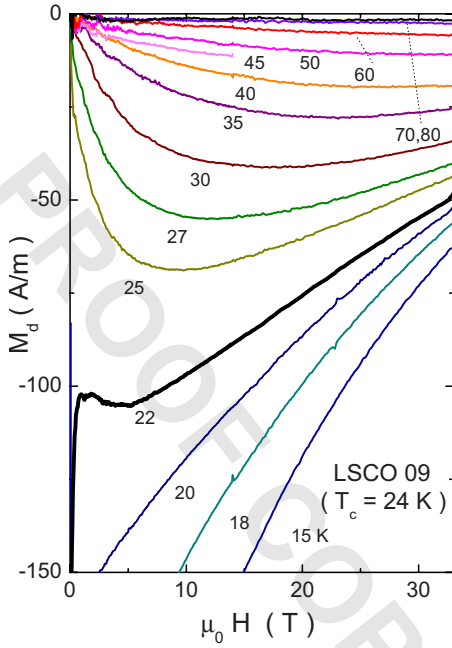


FIG. 2. (Color online) Magnetization curves M_d vs H in LSCO 09 measured in intense fields up to 33 T. T_c lies between the curves at 22 K (bold) and 25 K.

179 using a limited field range $H < 15$ T, this putative linear be-
 180 havior to a different mechanism (e.g., quasiparticles with
 181 Landau diamagnetism). Above T_c , M_d is inherently nonlinear
 182 in M up to the onset temperature T_{onset}^M , but one needs pro-
 183 gressively higher fields to see the nonlinearity as T increases.
 184 The diamagnetic M_d - H curves of sample LSCO 17
 185 ($x=0.17$, $T_c=38$ K) and sample LSCO 12 ($x=0.12$, T_c
 186 $=27$ K) measured in H up to 45 T are plotted in Figs. 3(a)
 187 and 3(b), respectively. In these higher-doped crystals, the
 188 pattern of the M_d - H curves is broadly similar to that in
 189 LSCO 09, and the foregoing discussion applies to the dia-
 190 magnetic curves. The higher field accessed (45 T) in Figs.
 191 3(a) and 3(b) confirms the intrinsic nonlinearity of $M_d(H)$. In

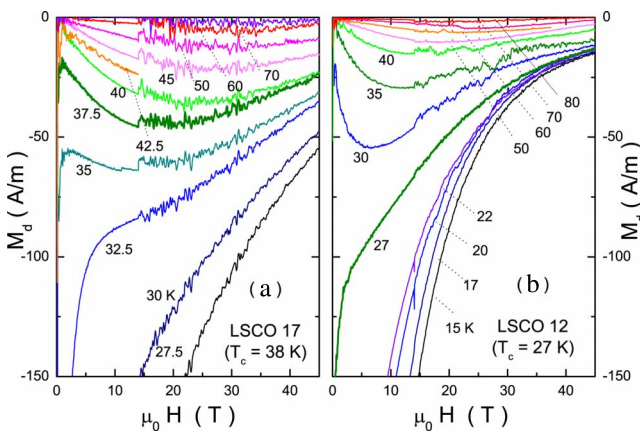


FIG. 3. (Color online) Comparison of magnetization curves M_d vs H in LSCO 17 and LSCO 12 measured in intense fields up to 45 T. Panel (a) shows curves for sample LSCO 17 ($x=0.17$ and $T_c=38$ K). Panel (b) displays curves of sample LSCO 12 ($x=0.12$ and $T_c=27$ K).

panel (a), M_d is manifestly nonlinear at all T up to 70 K,
 even though it seems linear when the field range is restricted
 to $H < 10$ T.

The magnitude of M_d in the high-field curves reveals an
 interesting difference (for $T < T_c$) between LSCO 17 and
 LSCO 12. The monotonic decrease in $|M_d|$ with H provides
 an estimate of the upper critical-field scale H_{c2} (by extrapo-
 lating $M_d \rightarrow 0$). Comparing LSCO 17 with LSCO 12, we see
 that the scale of $|M_d|$ above 20 T is 2–3 times larger in the
 former at the same H and T . However, the stronger curvature
 of M_d vs H in LSCO 12 implies that the decay of M_d is more
 gradual so that its H_{c2} is actually higher than that in LSCO
 17. In the related cuprate $\text{La}_{2-x}\text{Ba}_x\text{CuO}_4$, stripe formation at
 $x=\frac{1}{8}$ drives T_c to 4 K.²⁰ The “dip” in the T_c dome in the
 phase diagram of LSCO suggests that fluctuating stripes may
 also exist at $x=\frac{1}{8}$. If this is true, the M_d results suggest that
 fluctuating stripes reduce the overall pair condensate strength
 (compared with $x=0.17$) but allows it to survive to slightly
 larger fields.

IV. BISMUTH-BASED CUPRATES

The nonlinear diamagnetic signals above T_c are also ob-
 served in the single-layer Bi 2201 family. In this series, the
 transition temperature T_c is tuned by the La content y . The
 optimal T_c occurs at $y \sim 0.44$. Samples with $y > 0.44$ are UD
 while those with $y < 0.44$ are OV.

Figure 4 displays the diamagnetic M_d - H curves of the
 single-layer cuprate Bi 2201 samples in the UD region [panel
 (a) and (b)], in the optimally doped region (C), and in the
 OV region (D). Above T_c , the M_d - H curves in Bi 2201 are
 also similar to those in LSCO shown in Figs. 2 and 3, except
 that the magnitudes of M_d and field scales are slightly
 smaller in the former. Above T_c , M_d attains a broad mini-
 mum at fields below 20 T, and then approaches zero at H
 ≥ 40 T. Like the curves for LSCO in Figs. 2 and 3, the
 curvature of the low-field M_d - H curves changes from nega-
 tive to positive as T increases across T_c . As H is increased
 beyond 20 T, M_d is greatly suppressed. Above T_c , the com-
 plete suppression of M_d requires very high fields, compa-
 rable to those needed below T_c . Even in UD Bi 2201 with
 $y=0.7$, where T_c is quite low (12 K), the M_d curves are
 suppressed to zero at $H \sim 38$ –42 T at $T \leq 45$ K. Above
 T_{onset}^M (~ 50 K in this sample), M_d vanishes throughout our
 entire field range. The interesting weak-field region is dis-
 cussed under “fragile London rigidity.”

In Fig. 5, we compare the curves in OPT and UD bilayer
 Bi 2212 (panels (a) and (b), respectively). Relative to the
 single-layer Bi 2201, the amplitude $|M_d|$ in Bi 2212 attains
 much larger values and extend to higher field scales. By
 extrapolating the low- T M_d - H curves, we estimate that H_{c2}
 exceeds ~ 150 T (compared with 50–80 T for Bi 2201).

A. Fragile London rigidity

One of the most interesting features of the vortex-liquid
 state above T_c is the fragile London rigidity observable in the
 limit $H \rightarrow 0$. In Ref. 11, Li *et al.* discovered that over a broad

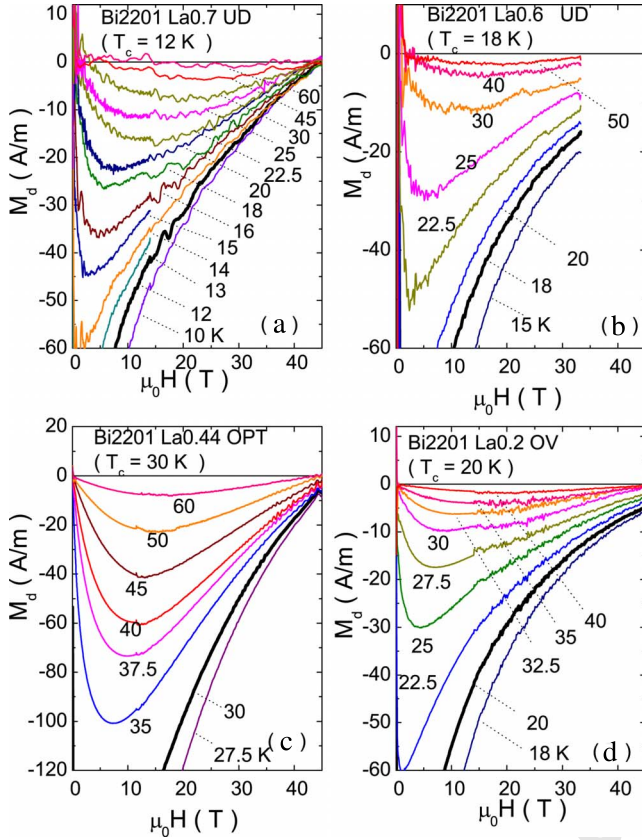


FIG. 4. (Color online) Curves of magnetization M_d vs H in Bi 2201 measured in intense fields. Panel (a) displays results on UD sample Bi 2201 (La content $y=0.7$ and $T_c=12$ K). Note that most of the results shown are at T above $T_c=12$ K. They approach zero at the same nominal field scale ~ 42 T. Panel (b) plots curves of M_d vs H measured in another UD Bi 2201 (La content $y=0.6$ and $T_c=18$ K). Panels (c) and (d) display M_d curves measured in optimally doped Bi 2201 (La content $y=0.44$ and $T_c=30$ K) and OV Bi 2201 (La content $y=0.2$ and $T_c=20$ K). In all these Bi 2201 samples, the curves of M_d vs H remain strikingly nonlinear high above T_c . In each panel, the curve closest to T_c is shown in bold. A preliminary version of panel (a) was published in Ref. 12.

246 interval of T (86–105 K) in OPT Bi 2212, the low- H M_d
247 follows the power-law dependence

$$248 \quad M_d(T, H) \sim -H^{1/\delta(T)} \quad (H \rightarrow 0) \quad (2)$$

249 with an exponent $\delta(T)$ that grows rapidly from 1 (at T
250 ≈ 105 K) to large values (>6) as $T \rightarrow T_c^+$. This implies that
251 the weak-field diamagnetic susceptibility $\chi = \lim_{H \rightarrow 0} M/H$
252 $\rightarrow -\infty$ is weakly divergent throughout the interval in T ,
253 where $\delta > 1$. However, this divergence is extremely sensitive
254 to field suppression. The fragile London rigidity seems to
255 reflect the increasing tendency of the phase-disordered con-
256 densate to establish long-range superfluid response as T
257 $\rightarrow T_c^+$. It has no analog in bulk samples of low- T_c supercon-
258 ductors but may exist in a finite- T interval above the
259 Kosterlitz-Thouless transition in 2D systems such as
260 $\text{Mo}_{1-x}\text{Ge}_x$ and InO_x .

261 Using a soft cantilever, we have observed a similar pattern
262 of magnetization in OPT Bi 2201. As shown in Fig. 6(a), the

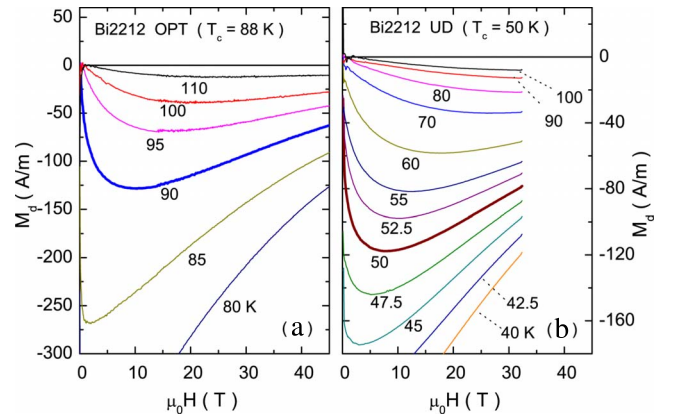


FIG. 5. (Color online) Comparison of high-field magnetization curves M_d vs H in OPT Bi 2212 and UD Bi 2212. Panel (a) (Ref. 12) displays the M_d curves in OPT Bi 2212 ($T_c=88$ K) in fields up to 45 T. Panel (b) plots magnetization curves in UD Bi 2212 ($T_c=50$ K) in fields up to 33 T. In each panel, the curve closest to T_c is shown in bold. Panel (a) is taken from Ref. 12.

M_d curves display increasingly strong curvature as H ap- 263
proaches zero from either direction. As T decreases from 38 264
K to T_c (30 K), the zero- H slope rises sharply to a vertical 265
line [see expanded scale in panel (b)]. The curve at T_c (bold 266
curve) seems to approach a logarithmic dependence vs H 267
(equivalent to $\delta \rightarrow \infty$). [As may be seen by the oscillations, 268
mechanical noise in this soft cantilever precludes accurate 269
measurements for $|H| < 300$ Oe. In Ref. 11, high-resolution 270
superconducting quantum interference device (SQUID) mag- 271
netometry was used to extend measurements down to 10 Oe 272
but the volume of the present Bi 2201 crystal is too small for 273
similar SQUID measurements.] Despite the lower resolution, 274
the divergent curvature apparent in Fig. 6 is consistent with 275
the appearance of fragile London rigidity starting 8 K above 276

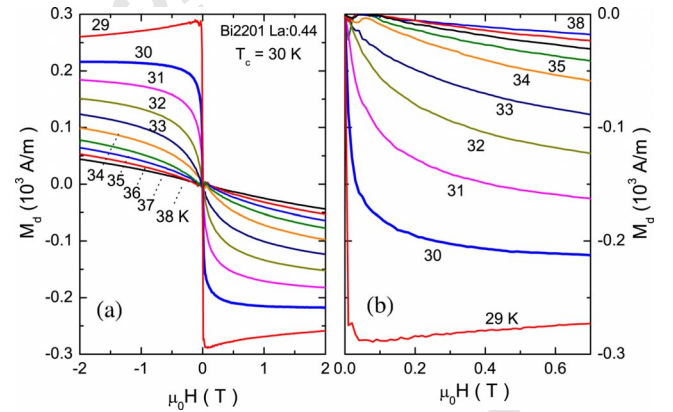


FIG. 6. (Color online) The low-field magnetization curves of OPT Bi 2201 (La content $y=0.44$). In (a), the striking weak-field nonlinearity is highlighted by displaying the variation in M_d from $H=-2$ to $+2$ T. Although $T_c=30$ K (bold curve), diamagnetism is observed up to the onset temperature $T_{onset}^M \approx 70$ K. Panel (b) shows the low-field curvature in expanded scale. The measurements were performed using a very soft cantilever beam. The divergent curvature of M_d at zero H is consistent with fragile London rigidity (Refs. 11 and 14).

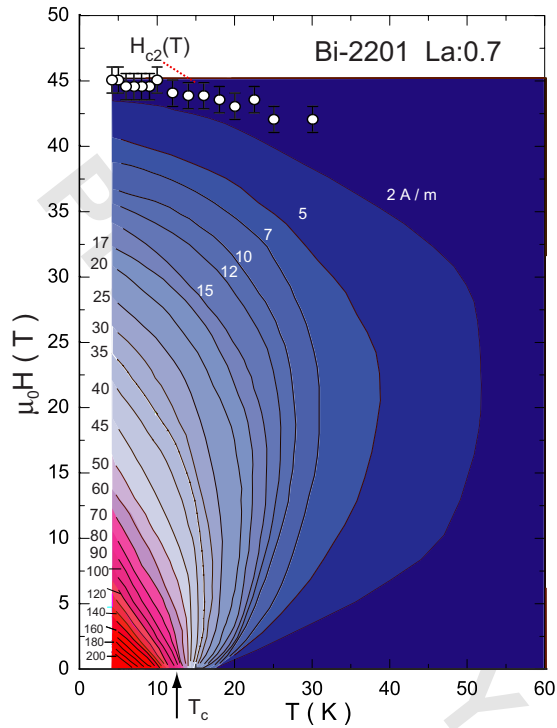


FIG. 7. (Color online) Contour plot of the diamagnetic magnetization $|M_d(T, H)|$ of UD Bi 2201 with La content $y=0.7$ and $T_c=12$ K (arrow). The spacing between adjacent contour lines is 10 A/m for $T < T_c$. The upper critical field H_{c2} (defined by extrapolating $M_d \rightarrow 0$) is plotted as open circles.

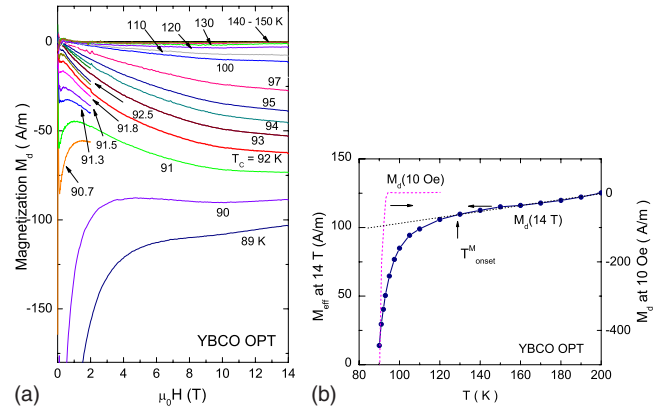


FIG. 8. (Color online) Magnetization curves of OPT $\text{YBa}_2\text{Cu}_3\text{O}_{7-\delta}$. Panel (a) displays curves of M_d vs H from $T=89$ to 150 K. Some curves were taken (at slower sweep rate) only to 1 T. Above $T_c=92$ K (bold curve), a sizeable diamagnetic signal persists to $T^M_{\text{onset}} \sim 130$ K. Panel (b) plots the T dependence of the observed M_{eff} with $H=14$ T. As in the other cuprates, M_{eff} may be fit to a straight line above the onset of the diamagnetic signal T^M_{onset} . The dashed curve is the Meissner signal M_{sq} measured by SQUID magnetometry with $H=10$ Oe.

If we fix T (e.g., at 4 K) and increase H , $|M_d|$ also decreases rapidly, as plotted in Fig. 4. The field H_{c2} ($=45$ T) at which $M_d \rightarrow 0$ is plotted as open circles. With increasing T , $H_{c2}(T)$ gradually decreases, roughly tracking the contour at 2 A/m. However, unlike the mean-field BCS scenario, H_{c2} remains very large at T_c (arrow). The magnetization contour plots in Bi 2212 (see Ref. 13) are roughly similar to that in Fig. 7. However, the scale of the magnitude $|M_d(T, H)|$ is much larger as expected. $M_d(T, H)$ also extends to much higher field scales. A particular feature is that, near T_c , the contours in OPT Bi 2212 are nearly vertical up to 33 T (the maximum applied field).¹³ This implies that, at the separatrix at T_s , M_d remains nearly H independent up to 33 T. By contrast, in Bi 2201, the constancy extends only to 10 T, as may be seen in Fig. 7.

V. OPTIMALLY DOPED YBCO

Optimally doped YBCO ($T_c=92$ K) is distinguished as the cuprate with the smallest resistivity anisotropy and the largest interlayer (c -axis) coupling energy. Because the coherence-length anisotropy $\xi_a/\xi_c=3-5$ is only moderate, the vortices have the largest stiffness modulus along c among cuprates (ξ_a and ξ_c are the coherence lengths along the axes a and c , respectively). Accordingly, the vortex-solid melting line $H_m(T)$ rises very rapidly below T_c (to ~ 15 T at 87 K). In the vortex-solid state ($H < H_m$), the dissipationless state survives to fields of 60 T or more. Optimally doped YBCO should be the least susceptible to the phase-disordering mechanism for the destruction of long-range phase coherence at T_c (and hence the best candidate for Gaussian fluctuations among cuprates).

However, the torque measurements reveal that T_c in OPT YBCO is also dictated by large phase fluctuations. Figure 8(a) displays the M_d - H curves in OPT YBCO (twinned)

277 T_c . The curves in Fig. 6(b) are remarkably similar to those
278 reported in Refs. 11 and 14 for OPT Bi 2212.
279 The fragile London rigidity is likely to extend over a
280 larger T interval in UD samples. However, it would be more
281 difficult to disentangle the intrinsic weak- H , nonlinear M_d - H
282 behavior from the effects of inhomogeneous broadening arising
283 from local variations in T_c . In OPT samples, we reason
284 that such effects are minimized. The bulk of the sample has
285 the maximum (OPT) T_c . Minority regions with lower T_c contribute
286 only negligibly to the screening current. Hence, observation of the
287 fragile state in OPT samples uncovers, in our opinion, a highly unusual
288 feature of cuprates that is intrinsic.

B. Contour plot

289 An instructive way to view the nonlinear diamagnetic magnetization
290 is the contour plot of M_d in the T - H plane.¹³ Figure 7 displays
291 the contour plot in single-layer UD Bi 2201 (La content $y=0.7$, $T_c=12$ K).
292 The value of $|M_d|$ is as indicated at selected contours. With H fixed
293 (e.g., at 10 T), $|M_d|$ decreases monotonically as T is raised from 4
294 to 60 K. Just as in the Nernst signal, the diamagnetic signal in the
295 T - H plane bulges out to temperatures high above T_c , with no
296 obvious discontinuities or changes in slope. The highest temperature
297 at which M_d is resolved is ~ 50 K (the onset temperature in this
298 sample). The absence of a boundary at T_c implies that the vortex-
299 liquid state below T_c evolves continuously to the diamagnetic state
300 above T_c .
301
302

336 measured to 14 T. The curves are broadly similar to those in
 337 LSCO 17 and OPT Bi 2212, except for the larger magnitude
 338 of $|M_d|$ (at comparable H and T). At $T_c=92$ K, $|M_d|$ reaches
 339 the substantial value ~ 60 A/m at 14 T (by contrast, it
 340 should be nearly unobservable in a Gaussian mean-field pic-
 341 ture). Over the broad interval $92 \rightarrow 130$ K, a large diamag-
 342 netic signal is easily observed. As in the other hole-doped
 343 cuprates, very intense fields are needed to suppress M_d in
 344 this interval.

345 In (b), we plot the T dependence of the total torque mag-
 346 netization M_{eff} observed at 14 T (solid circles). As in the
 347 other hole-doped cuprates, M_{eff} is unresolved from the Van
 348 Vleck line $(A+BT)H$ until T reaches $T_{onset}^M \sim 130$ K (arrow),
 349 below which it accelerates to very large negative values. For
 350 comparison, we have also plotted the magnetization mea-
 351 sured in a very weak $H \sim 10$ Oe (dashed curve) using a
 352 SQUID magnetometer. The nearly vertical decrease signals
 353 flux expulsion at T_c . We remark that, although M_d , measured
 354 with $H=10$ Oe, is virtually unresolvable above T_c , the dia-
 355 magnetic susceptibility χ is actually quite large above T_c [as
 356 is clear from panel (a)]. Because M_d is robust to intense H
 357 (100 T), the curve at 14 T reveals the existence of the large
 358 fluctuating diamagnetism associated with the vortex liquid.
 359 This point, emphasized in Refs. 10 and 11, highlights the
 360 major difference between the diamagnetism in hole-doped
 361 cuprates and low- T_c superconductors. In the latter, increasing
 362 H in the fluctuation regime above T_c rapidly squelches the
 363 (Gaussian) fluctuation signal altogether. The curves in Fig.
 364 8(a) displaying significant diamagnetism surviving to intense
 365 fields, at temperatures up to 40 K above T_c is strong evidence
 366 that we are observing the phase-disordering mechanism,
 367 rather than Gaussian mean-field fluctuations. A comparison
 368 of the Nernst and magnetization signals in UD YBCO is
 369 given in Ref. 24.

370 VI. ONSET TEMPERATURES AND PHASE DIAGRAM

371 An important question is how high in temperature does
 372 the diamagnetic signal extend above T_c . Following the pro-
 373 cedure in Wang *et al.*,¹⁰ we have plotted the total effective
 374 magnetization M_{eff} measured in fixed H (14 T) versus T .
 375 Figure 9 displays these plots for several samples of Bi 2201
 376 [panel (a)] and LSCO [panel (b)]. In agreement with the
 377 results for Bi 2212 in Ref. 10, M_{eff} displays a weak T de-
 378 pendence at elevated T that may be fitted to the Van Vleck
 379 anisotropy term $\Delta\chi_p=A+BT$ (straight lines). The anisotropy
 380 $\Delta\chi_p$ leads to a paramagnetic torque background, as dis-
 381 played. In each sample, $M_{eff}(T)$ displays a sharp downward
 382 deviation, beginning at the temperature defined as T_{onset}^M (ar-
 383 rows). This reflects the appearance of local supercurrents in-
 384 duced in response to the applied field. While feeble near
 385 T_{onset}^M , the diamagnetic term $M_d(T)$ grows very rapidly in
 386 magnitude to pull M_{eff} to large negative values.

387 To determine T_{onset}^M with reasonable accuracy, it is impor-
 388 tant to establish the Van Vleck term χ_p with a sufficiently
 389 dense set of points above T_{onset}^M . At elevated temperatures, the
 390 magnetization curves become closely spaced. Thus, the sta-
 391 bility of the cantilever as well as the resolution in measuring
 392 M_{eff} must be sufficiently high to allow adjacent curves to be

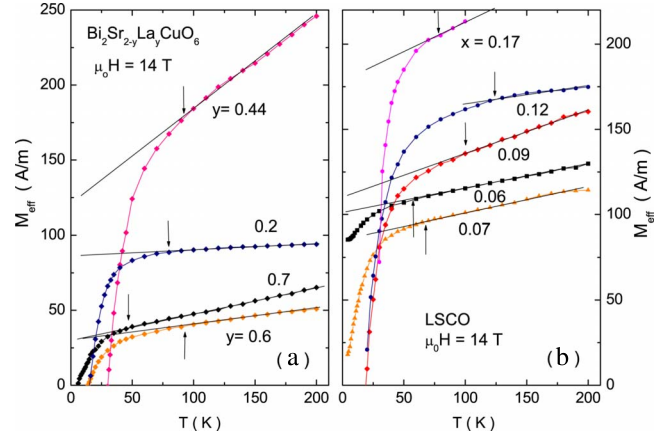


FIG. 9. (Color online) Plots of the temperature dependence of $M_{eff}(T)$ in Bi 2201 (a) and in LSCO (b), showing the onset of diamagnetism as T is decreased. In both panels, the value of M_{eff} measured at $H=14$ T is plotted vs T in samples with various doping levels x . In general, M_{eff} at high T varies weakly vs T , as shown by the straight lines which are of the form $A+BT$. Relative to this linear background, M_{eff} shows a strong downwards deviation starting at the onset temperature T_{onset}^M (indicated by arrows).

distinguished. As examples, we display in Figs. 10(a) and 393
 10(b) expanded views of the curves in LSCO 09 and LSCO 394
 12, respectively. The values of M_{eff} at $H=14$ T are the ones 395
 plotted in Fig. 9. 396

The profile of M_{eff} vs T is common to all the samples 397
 investigated, even those in the extreme UD regime. The char- 398
 acteristic profile is qualitatively different from that seen in 399
 the Gaussian regime in BCS superconductors. Remarkably, 400
 the rapid downward acceleration of the diamagnetic signal 401
 matches the equally rapid growth of the Nernst signal taken 402
 at 14 T (Fig. 3 in Ref. 10 compares the profiles of the Nernst 403
 signal and M_d measured in the same crystal of Bi 2212). 404

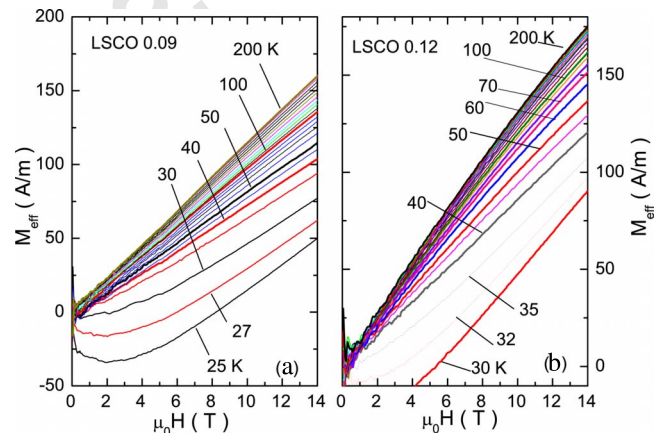


FIG. 10. (Color online) Expanded view of the total observed magnetization M_{eff} vs H in LSCO 09 (a) and LSCO 12 (b). Above T_{onset}^M , the T dependence of the curves is only from the paramagnetic Van Vleck term. Below T_{onset}^M , however, the diamagnetic term M_d grows rapidly to dominate the T dependence. The stability of the torque cantilever and the resolution in τ are sufficient to allow closely spaced curves to be resolved. The uncertainty in measuring M_{eff} makes the largest contribution to the error bars in T_{onset}^M .

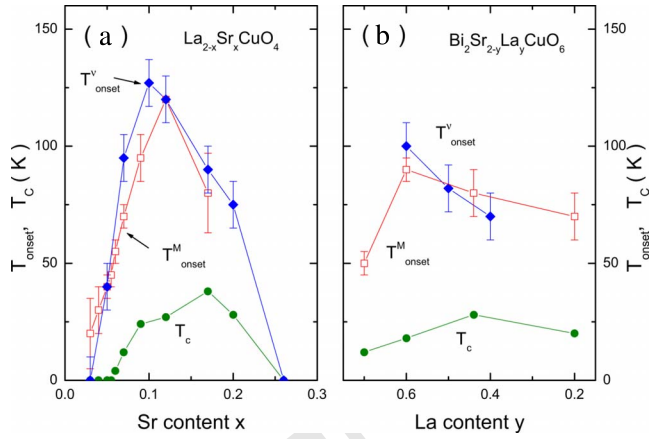


FIG. 11. (Color online) Phase diagram comparing the onset temperatures for the Nernst and diamagnetism signals vs doping x in $\text{La}_{2-x}\text{Sr}_x\text{CuO}_4$ (a) and in $\text{Bi}_2\text{Sr}_{2-y}\text{La}_y\text{CuO}_6$ (b). The superconducting transition temperature T_c (solid circles) is plotted with the onset temperature T_{onset}^v determined by the Nernst effect (solid diamonds) and T_{onset}^M determined by torque magnetometry (open squares). In panel (b) for $\text{Bi}_2\text{Sr}_{2-y}\text{La}_y\text{CuO}_6$, a large La content y implies small hole carrier concentration (UD regime).

405 To compare T_{onset}^M obtained here with the onset tempera-
 406 ture of the vortex Nernst signal T_{onset}^v ,² we plot the two onset
 407 temperatures vs doping x in the phase diagram for LSCO
 408 [Fig. 11(a)] and Bi 2201 [Fig. 11(b)]. Remarkably, in LSCO,
 409 T_{onset}^M (open squares) is nominally equal to T_{onset}^v in LSCO
 410 over the entire doping range investigated. The major differ-
 411 ence is that the former seems to peak at $x=0.12$ whereas the
 412 latter peaks at 0.10. The error bars at both temperatures are
 413 too large to determine if the disagreement is real. In the
 414 interesting UD side, both temperatures decrease roughly lin-
 415 early with x as $x \rightarrow 0$. (In an earlier analysis,² T_{onset}^v was
 416 extrapolated below $x=0.05$ to reach 0 at $x=0.03$. Our recent
 417 results show that this extrapolation is incorrect. Because the
 418 Nernst signal at $x=0.03$ is too weak to resolve even at low T ,
 419 there is actually no experimental information on T_{onset}^v . By
 420 contrast, the results on M_{eff} vs T [Fig. 9(b)] allow T_{onset}^M to be
 421 fixed reliably at small x .) Interestingly, the x dependence of
 422 H_{c2} obtained in Ref. 15 is also linear in x in this regime.

423 In Bi 2201 [panel (b)], the two temperature scales are also
 424 quite similar. However, the trend of T_{onset}^v on the OV side
 425 appears to be slightly steeper than that of T_{onset}^M . A caveat is
 426 that the torque measurements here were not performed on the
 427 same crystals as the Nernst experiments.

428 For the equivalent phase diagram of Bi 2212, see Ref. 10.
 429 The phase diagram for YBCO appears in Ref. 24.

430 VII. DISCUSSION

431 A. Diamagnetism and supercurrent response

432 The presence of a large diamagnetic response that is both
 433 strongly T dependent and nonlinear in H deeply implicates
 434 Cooper pairing. Diamagnetism involves an orbital current
 435 density \mathbf{J} that is antiparallel to the applied vector potential \mathbf{A}
 436 (as in the London equation). Cooper pairing is—to our
 437 knowledge—the only established electronic state capable of

generating the current response consistent with the nonlinear,
 strongly T -dependent diamagnetism reported here. [Core dia-
 magnetism in insulators and Landau diamagnetism (observed
 in pure Bi) are both strictly H linear to extremely large H
 ($\mu_B H \approx W$, where W is the bandwidth and μ_B the Bohr mag-
 neton) and nearly T independent. A “superdiamagnetic” state
 based on toroidal, orbital moments has been theorized²¹ but
 this state has never been observed.] Hence, diamagnetism
 provides a rather direct detector of incipient Cooper pairing
 in the cuprates.

As shown in Secs. III–V for LSCO, the Bi-based cuprates
 and YBCO, respectively, the M_d - H curves above T_c show
 similar patterns—a broad minimum in moderate fields fol-
 lowed by a steady suppression to zero in very high fields.
 This pattern evolves continuously from the curves measured
 below T_c , which display a divergence at low field caused by
 the Meissner effect. Above T_c , this divergence vanishes be-
 cause of the loss of long-range phase coherence. Nonethe-
 less, a reduced local phase rigidity survives,¹¹ which gives
 rise to the enhanced diamagnetic M_d above T_c at low fields.
 Although its overall magnitude is ~ 10 times smaller than
 below T_c (when observed at similar H), M_d is readily de-
 tected as a strongly T -dependent and H -nonlinear response.
 In UD Bi 2201, we have accomplished full field suppression
 of M_d in fields ~ 45 T. However, in all other cuprates, the
 full suppression requires fields in excess of 80 T (possibly as
 high as 150 T). These impressively large field scales are a
 consequence of the anomalously large binding energies of
 Cooper pairs in hole-doped cuprates. The broad similarity of
 the magnetization curves in LSCO, Bi 2201, Bi 2212, and
 YBCO suggests that the diamagnetic behavior above T_c is
 universal in the hole-doped cuprates. They are qualitatively
 different from the diamagnetic response in low- T_c supercon-
 ductors.

It is instructive to compare the diamagnetism in cuprates
 with the fluctuating diamagnetism observed in disordered
 MgB_2 . In a recent experiment, Bernardi *et al.*²² compared the
 magnetization of pure MgB_2 ($T_c=39$ K) with disordered
 $\text{Mg}_{1-x}\text{B}_2\text{Al}_x$ ($x=0.25$, $T_c=25$ K). In the disordered sample
 (which has a broad transition width of ~ 15 K), the curves of
 M_d vs H show that sizeable diamagnetism exists in the nar-
 row interval 28–32 K above its T_c (Fig. 5 of Ref. 22). The
 profile of M_d vs H , which displays a broad minimum at
 ~ 200 Oe, is roughly similar to the profiles reported here
 (aside from the field scale). The broad transition width im-
 plies large inhomogeneities in the Al distribution. As the dia-
 magnetic response above T_c does not persist above T_c of pure
 MgB_2 (39 K), we suggest that the fluctuation diamagnetism
 arises from Al-poor regions of MgB_2 which have the highest
 T_c . Thus, over the whole sample, diamagnetism is observable
 above 25 K, but not above 39 K. This contrasts with the
 cuprates. In the OPT sample within each family, T_{onset}^M
 extends above T_c by factors of 1.3 (YBCO), 1.4 (Bi 2212), 2.1
 (LSCO), and 2.5 (Bi 2201). Clearly, we cannot simply ex-
 plain away the high- T diamagnetism as coming from isolated
 OPT regions with the highest T_c . The comparison shows that
 the local supercurrents detected in MgB_2 arise from isolated
 regions with strong amplitude fluctuations and a broad dis-
 tribution of local T_c 's. By contrast, the diamagnetic signal in
 cuprates arises from a condensate that has lost phase stiff-

ness, even though the gap amplitude remains large and nominally uniform above T_c .

B. Quasiparticle term in Nernst signal

In UD LSCO, the quasiparticle (qp) current makes a significant contribution to the Nernst signal e_N . In the initial report of Xu *et al.*,¹ the onset temperature T_ν was found to remain high even when x falls below 0.1 ($T_\nu \sim 150$ K for $x=0.05$). This was traced² to a significant qp contribution to the Nernst signal. To discuss the qp term, it is crucial to consider the *sign* of the Nernst effect.

By convention, the sign of the Nernst effect is defined as that of the triple product $\mathbf{E}_N \cdot \mathbf{H} \times (-\nabla T)$ with \mathbf{E}_N the observed Nernst E field.⁵ This rule is equivalent to the old convention based on “amperian” current direction (clearly described by Bridgman²³). For vortices, $\mathbf{E}_N = \mathbf{B} \times \mathbf{v}_L$, where the vortex line velocity \mathbf{v}_L is $\parallel(-\nabla T)$. Hence vortex flow produces a positive Nernst signal. The qp contribution may have either sign (unrelated to their charge sign).

When the qp term is negative, it is relatively easy to separate the two contributions, especially by going to intense H . However, if the qp term is positive, the separation is more difficult. In Ref. 2, Wang *et al.* introduced a method for separating the qp and vortex terms by simultaneous measurements of the Hall angle θ_H and thermopower S vs H to obtain the term $S \tan \theta_H$. This subtraction procedure yields the onset temperature T_{onset}^ν for the vortex term (45 K at $x=0.05$), which is plotted in Fig. 11(a). With the qp subtraction applied to the samples $x \leq 0.07$, the curve of T_{onset}^ν vs x has a tilted dome profile with a sharp peak at $x=0.125$. For OPT and OV LSCO, Wang *et al.* found⁵ that the qp term is negative and negligible compared with the vortex term. Hence, T_{onset}^ν gives the onset of the vortex term without the need for corrections. [The qp term is also negative in YBCO, Bi 2201, and Bi 2212 (Ref. 5)].

Recently, this assumption has been challenged by Cyr-Choiniere *et al.*,¹⁸ who proposed that rearrangement of the FS, possibly by charge ordering or stripe formation, produces a positive quasiparticle term that dominates the Nernst signal over the LSCO phase diagram at high temperatures. Although their Nernst measurements were largely on Eu-doped and Nd-doped LSCO where static stripes are experimentally observed, they have extended their hypothesis to pure LSCO. There, they proposed that a positive qp also accounts for its Nernst signal at elevated T (except in a narrow interval just above T_c).

In the scenario of Ref. 18, the onset temperature for vortex fluctuations should lie considerably lower than the dome of T_{onset}^ν plotted in Fig. 11(a). However, the good agreement between T_{onset}^M and T_{onset}^ν shows that this is not the case. As we argued above, the strongly T - and H -dependent diamagnetism arises only from the pair condensate, and is unaffected by qp contributions. The agreement between T_{onset}^M and T_{onset}^ν seems to us to be strong evidence against the proposal in Ref. 18, at least in pure LSCO. For the claim to be viable, the hypothetical quasiparticles would have to produce a large, T -dependent diamagnetism that is also strongly nonlinear in H , as well as a positive Nernst signal.

The hypothesis of Cyr-Choiniere *et al.*¹⁸ is the latest of several proposals (see discussion in Ref. 5) that have sought to explain away the unexpected Nernst signal in the cuprates by invoking quasiparticles with *ad hoc* properties. Are the large Nernst signals at high T from vortices in a phase-disordered condensate or from qp? We argue that torque magnetometry and the Nernst effect together constitute an incisive combination that answers this question. When the two probes show that a large positive Nernst signal coexists with a diamagnetic susceptibility (with the same onset temperatures and similar profiles vs T and H), the case in favor of phase slippage in a pair condensate with strongly disordered phase seems compelling to us. This is one of our main conclusions.

The magnetization Nernst approach can also be turned around to identify situations when the Nernst signal is not caused by vorticity. As mentioned, in UD LSCO ($x < 0.07$) the agreement of T_{onset}^M and T_{onset}^ν provides confirmation that the subtraction procedure based on $S \tan \theta_H$ (Ref. 2) is valid. (In the broad interval between T_{onset}^M and T_ν , extending from 45 to 150 K for $x=0.05$, there is a large positive Nernst signal, but diamagnetism is absent. Thus, even if the qp contribution had not been identified,² the present experiment would have detected the correct onset of the vortex term.)

In UD YBCO, the qp Nernst signal is unusually large in a narrow window of doping. In this doping range, when the qp term appears at high T , it is negative as in OV LSCO. Significantly, the diamagnetic signal is absent until the vortex Nernst signal appears at a lower T (detailed YBCO results are reported in Ref. 24). Hence, when used together, the torque magnetization and Nernst effect readily distinguish qp from vortex contributions to the Nernst signal. Nernst effect and diamagnetism studies on $\text{La}_{2-x}\text{Ba}_x\text{CuO}_4$ (Ref. 20) should provide valuable insight into the fluctuation regime in which stripes coexist with Cooper pairing.

C. Related experiments

The surviving pair condensate above T_c has also been observed in other experiments, notably in measurements of the kinetic inductance,²⁵ scanning tunnel microscope experiments on the gap above T_c ,²⁶ and survival of Bogolyubov quasiparticles above T_c .²⁷ Consistent with these observations, our results imply that the pair condensate exists well above T_c , surviving as a dilute vortex liquid with local phase rigidity of short phase-correlation length. A number of groups recently calculated the Nernst signal and diamagnetism above T_c in 2D superconductors and applied the results to cuprates.^{28–32} The vortex liquid viewed as an incompressible superfluid has been treated by Anderson.^{33,34} A relevant discussion of the relation of the quantum oscillation results to the Nernst and magnetization results is given in Ref. 35.

To summarize, the high-field torque magnetometry measurements reveal that the diamagnetism persists well above T_c in several families of hole-doped cuprates. As a strongly nonlinear M_d vs H is characteristic of local supercurrent response, the diamagnetism is direct evidence that the pair condensate exists above T_c , surviving in places all the way to T_{onset}^M . Hence, phase slippage is the origin of the large Nernst

612 effect signals observed to that temperature. The agreement
613 between the onset temperatures T_{onset}^V and T_{onset}^M precludes
614 quasiparticle interpretations for the positive Nernst signal
615 above T_c . The magnetization results pose very serious diffi-
616 culties for the quasiparticle hypothesis¹⁸ proposed recently
617 for the Nernst effect in pure LSCO
618 *Note added in proof.* Two recent papers are pertinent to
619 the issues discussed here [36 and 37].

620 ACKNOWLEDGMENTS

621 We acknowledge numerous helpful discussions with P. W.

633
634
635

- 636 ¹Z. A. Xu, N. P. Ong, Y. Wang, T. Kakeshita, and S. Uchida,
637 Nature (London) **406**, 486 (2000).
638 ²Y. Wang, Z. A. Xu, T. Kakeshita, S. Uchida, S. Ono, Y. Ando,
639 and N. P. Ong, Phys. Rev. B **64**, 224519 (2001).
640 ³Y. Wang, N. P. Ong, Z. A. Xu, T. Kakeshita, S. Uchida, D. A.
641 Bonn, R. Liang, and W. N. Hardy, Phys. Rev. Lett. **88**, 257003
642 (2002).
643 ⁴Y. Wang, S. Ono, Y. Onose, G. Gu, Y. Ando, Y. Tokura, S.
644 Uchida, and N. P. Ong, Science **299**, 86 (2003).
645 ⁵Y. Wang, L. Li, and N. P. Ong, Phys. Rev. B **73**, 024510 (2006).
646 ⁶V. J. Emery and S. A. Kivelson, Nature (London) **374**, 434
647 (1995).
648 ⁷C. Capan, K. Behnia, J. Hinderer, A. G. M. Jansen, W. Lang, C.
649 Marcenat, C. Marin, and J. Flouquet, Phys. Rev. Lett. **88**,
650 056601 (2002).
651 ⁸F. Rullier-Albenque, R. Tourbot, H. Alloul, P. Lejay, D. Colson,
652 and A. Forget, Phys. Rev. Lett. **96**, 067002 (2006).
653 ⁹F. Rullier-Albenque, H. Alloul, C. Proust, P. Lejay, A. Forget,
654 and D. Colson, Phys. Rev. Lett. **99**, 027003 (2007).
655 ¹⁰Y. Wang, L. Li, M. J. Naughton, G. D. Gu, S. Uchida, and N. P.
AQ: #56 Ong, Phys. Rev. Lett. **95**, 247002 (2005).
3 657 ¹¹L. Li, Y. Wang, M. J. Naughton, S. Ono, Y. Ando, and N. P. Ong,
658 Europhys. Lett. **72**, 451 (2005).
AQ: #59 659 ¹²L. Li, Y. Wang, J. G. Checkelsky, M. J. Naughton, S. Komiya, S.
4 660 Ono, Y. Ando, and N. P. Ong, Physica C **460-462**, 49 (2007).
661 ¹³L. Li, Y. Wang, M. J. Naughton, S. Komiya, S. Ono, Y. Ando,
662 and N. P. Ong, J. Magn. Magn. Mater. **310**, 460 (2007).
663 ¹⁴N. P. Ong, Y. Wang, L. Li, and M. J. Naughton, Phys. Rev. Lett.
664 **98**, 119702 (2007).
665 ¹⁵L. Li, J. G. Checkelsky, S. Komiya, Y. Ando, and N. P. Ong, Nat.
666 Phys. **3**, 311 (2007).
667 ¹⁶D. C. Johnston and J. H. Cho, Phys. Rev. B **42**, 8710 (1990).
668 ¹⁷A. Lascialfari, A. Rigamonti, L. Romano', A. A. Varlamov, and
669 I. Zucca, Phys. Rev. B **68**, 100505(R) (2003).
670 ¹⁸O. Cyr-Choinière, R. Daou, F. Laliberté, D. LeBoeuf, N. Doiron-

Anderson, J. C. Davis, S. A. Kivelson, P. A. Lee, T. Senthil, 622
Z. Tešanović, and A. Yazdani. The research at Princeton is 623
supported by funds from U.S. National Science Foundation 624
under the MRSEC Grants No. DMR-0213706 and No. 625
DMR-0819860. Y.W. is supported by NSFC and MOST of 626
China. G.D.G. is supported by the Department of Energy 627
(DOE) under Contract No. DE-AC02-98CH10886. The high- 628
field experiments were performed at the National High Mag- 629
netic Field Laboratory, which is supported by NSF Coopera- 630
tive Agreement No. DMR-084173, by the State of Florida, 631
and by the DOE. 632

- Leyraud, J. Chang, J.-Q. Yan, J.-G. Cheng, J.-S. Zhou, J. B. 671
Goodenough, S. Pyon, T. Takayama, H. Takagi, Y. Tanaka, and 672
L. Taillefer, Nature (London) **458**, 743 (2009). 673 AQ
674 #5
¹⁹C. Bergemann, A. W. Tyler, A. P. Mackenzie, J. R. Cooper, S. R. 675
Julian, and D. E. Farrell, Phys. Rev. B **57**, 14387 (1998). 676
²⁰Q. Li, M. Hucker, G. D. Gu, A. M. Tsvelik, and J. M. Tranquada, 677
Phys. Rev. Lett. **99**, 067001 (2007). 678
²¹V. L. Ginzburg, A. A. Gorbatshevich, Yu. V. Kopayev, and B. A. 679
Volkov, Solid State Commun. **50**, 339 (1984). 680
²²E. Bernardi, A. Lascialfari, A. Rigamonti, and L. Romano', 681
Phys. Rev. B **77**, 064502 (2008). 682
²³P. W. Bridgman, Phys. Rev. **24**, 644 (1924). 683 AQ
²⁴M. Liu, Y. Wang, L. Li, and N. P. Ong (unpublished). 684 #6
²⁵J. Corson, R. Mallozzi, J. Orenstein, J. N. Eckstein, and I. Bo- 685
zovic, Nature (London) **398**, 221 (1999). 686
²⁶K. K. Gomes, A. N. Pasupathy, A. Pushp, S. Ono, Y. Ando, and 687
A. Yazdani, Nature (London) **447**, 569 (2007). 688
²⁷J. Lee, K. Fujita, A. R. Schmidt, C. K. Kim, H. Eisaki, S. 689
Uchida, and J. C. Davis, Science **325**, 1099 (2009). 690
²⁸L. Benfatto, C. Castellani, and T. Giamarchi, Phys. Rev. Lett. **98** 691 AQ
117008 (2007); **99**, 207002 (2007). 692 #7
²⁹C. Jooss and V. Born, Phys. Rev. B **73**, 094508 (2006). 693 AQ
³⁰Z. Tešanović, Nat. Phys. **4**, 408 (2008). 694 #8
³¹D. Podolsky, S. Raghu, and A. Vishwanath, Phys. Rev. Lett. **99**, 695
117004 (2007). 696
³²S. Mukerjee and D. A. Huse, Phys. Rev. B **70**, 014506 (2004). 697
³³P. W. Anderson, Nat. Phys. **3**, 160 (2007). 698
³⁴P. W. Anderson, Phys. Rev. Lett. **100**, 215301 (2008). 699
³⁵T. Senthil and P. A. Lee, Phys. Rev. B **79**, 245116 (2009). 700
³⁶R. Daou, J. Chang, D. LeBoeuf, O. Cyr-Choinière, F. Laliberté, 701
N. Doiron-Leyraud, B. J. Ramshaw, R. Liang, D. A. Bonn, W. 702
N. Hardy and L. Taillefer, arXiv:0909.4430, Nature (to be pub- 703
lished). 704
³⁷A. Hackl and M. Vojta, arXiv:0909.4534, Phys. Rev. B (to be 705
published).

AUTHOR QUERIES —

- #1 AU: Please verify the changes made in Affiliation 5.
- #2 AU: Please note change to figures sublabels from "(A), (B), (C), (D)" to "(a), (b), (c), (d)" as per journal style. Please check and verify changes in text as well.
- #3 Au: Please check changes to Refs. 10 and 29.
- #4 AU: Please check reference for content flaws
- #5 Au: Ref. 18 has been expanded. Please check and verify. Also the first author should be 'Cyr-Choinière' not 'Cyr-Choiniere' in Ref. 18. Please verify.
- #6 Au: Please update Ref. 24 if possible.
- #7 Au: The year should be '2007' not '2009' in Ref. 28b. Please verify.
- #8 Au: The volume should be '4' not '5' in Ref. 30. Please verify.